

# Flowers in flour: avalanches in cohesive granular matter.

E. Freyssingéas, M.-J. Dalbe and J.-C. Géminard

*Université de Lyon, Laboratoire de Physique, Ecole Normale Supérieure de Lyon, CNRS, 46 Allée d'Italie, 69364 Lyon cedex 07, France.*

We report on the intermittent dynamics of the free surface of a cohesive granular material during a silo discharge. In absence of cohesion, one observes the formation and the growth of a conical crater whose angle is well-defined and constant in time. When the cohesion is involved, the free surface exhibits a complex dynamics and the crater, resulting from a series of individual avalanches, is no longer axi-symmetric. However, in spite of the intermittent behavior of the free surface, the flow-rate is observed to remain constant throughout the discharge.

## INTRODUCTION

The flow of granular media through an orifice, because of its practical importance, has been intensely studied in the last 50 years [1–11]. The phenomenon also presents some interesting fundamental features. For instance, what mainly differentiates the discharge of a container filled with granular matter from one filled with a viscous liquid is that the mass flow rate does not depend on the height of material above the outlet. The explanation most frequently used for this independence is based on the Janssen effect: the distribution of the weight of the material onto the silo walls, due to the friction forces, leads to a saturation of the pressure at the bottom, which results in a constant flow rate [12]. As we shall see, even if the conditions for the Janssen effect to be involved are not fulfilled, the flow rate remains constant because it is independent of the pressure in the outlet region [13]. In general, the discharge of a silo through an orifice can present three regimes: a continuous flow, an intermittent flow, or a complete blockage of the flow due to arching depending on the ratio of the typical grain diameter  $d$  to the aperture diameter  $D$  [14–16]. However, for a large outlet, in the continuous regime, the mass flow rate  $Q$  is satisfactorily accounted for by the empirical Beverloo law which, for instance, predicts that  $Q \propto D^{5/2}$  [1, 17].

In addition, adding even minute amounts of liquid can change dramatically the mechanical properties of the granular matter. For instance, during the building of sand castles, one observes a transformation from a fluid-like to a sticky and deformable material with increasing water content. Indeed, at very low water content, the formation of partially developed capillary bridges leads to a fast increase of tensile strength whereas, for large enough fluid content, tensile strength is nearly constant [18]. Cluster formation was identified as the main mechanism responsible of such a behavior [19]. Depending on the granular system, the cohesion can be due to electrostatic interactions and van der Waals forces, magnetic interactions [20], and even solid bonds [21, 22]. The cohesion has been lately proven to give rise to puzzling surface patterning when the material is deformed [23].

Suprisingly, among the broad literature about the silo

discharge, only a few studies were dedicated to the case of cohesive materials and the dynamics of the free surface has not yet been reported. In the present article, we report a study of the surface dynamics during the continuous discharge of a weakly cohesive material and show that it exhibits a complex and interesting behavior.

## EXPERIMENTAL TECHNIQUES

### Experimental principle

We aim at assessing the deformation of the free surface of a granular material during a silo discharge. To do so, we consider the flow of a granular material through an orifice pierced at the base of a cylindrical container. The flow-rate is measured and the free surface is observed so as to determine its geometry.

First, it is a common observation that the discharge leads to a significant deformation of the free surface only when the height of the granular column compares with the diameter of the container. In our experimental conditions, the diameter of the container is always larger than the depth of the granular bed. We note that, in this limit, the granular column is not subjected to any dynamical version of the usual static Janssen effect [3] and the pressure at the outlet thus continuously decreases during the discharge [24]. Second, it has long been identified that fluctuations of the outflow and, even, blockages are observed if the diameter of the outlet is too small, typically less than ten times the grains diameter [25]. In order to avoid system blockages, the diameter of the aperture is at least ten times the diameter of the grains in our experimental conditions. At last, we consider the case of slightly cohesive granular matter, meaning that the angle of avalanche is less than 90 degrees. The cohesion is tuned by considering various grain sizes, whereas the typical atmospheric conditions remain constant. The cohesion is accounted for by the measurement of the angle of avalanche [26, 27].

Thus, in brief, the experiment consists in studying the discharge of a wet granular material through a hole pierced at the bottom of a bucket.

## Experimental setup

The experimental setup (Fig. 1) consists of a cylindrical container with a hole at the bottom. The upper surface is observed thanks to two CCD cameras whereas the flow-rate is measured by means of a scale placed underneath.

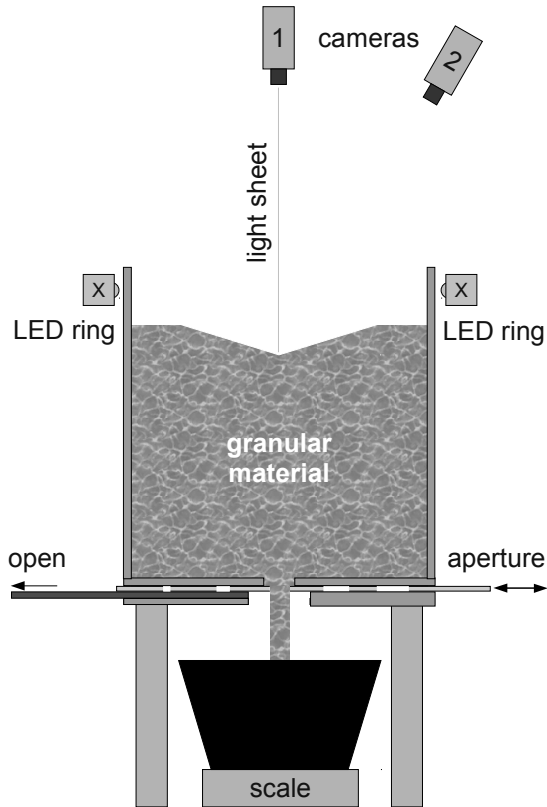


FIG. 1. **Experimental setup** – The experimental setup consists of a cylindrical container with a hole at the bottom. The mass of the falling grains is measured by means of a scale placed underneath whereas the deformations of the free surface are observed thanks to two CCD cameras. A ring of LEDs is used to obtain a good contrast in the images from above. A LASER diode is used to produce a light sheet which makes possible to report the surface profile in a vertical, radial, plane. Two thin lamina, located at the base of the container are used to tune the size of the aperture and to open the container (see text for details).

The container is made of a Plexiglas cylinder (inner diameter 15 cm, height 15 cm) glued on a Plexiglas plate (Fig. 1) supported by four vertical legs. A large orifice (diameter 1 cm) is drilled in the plate at the center. Two additional lamina sliding in a slot (width 2 cm) are used to tune (Fig. 1, aperture) the diameter  $D$  of outlet (2, 4, 6 or 8 mm) and to suddenly initiate the flow (Fig. 1,

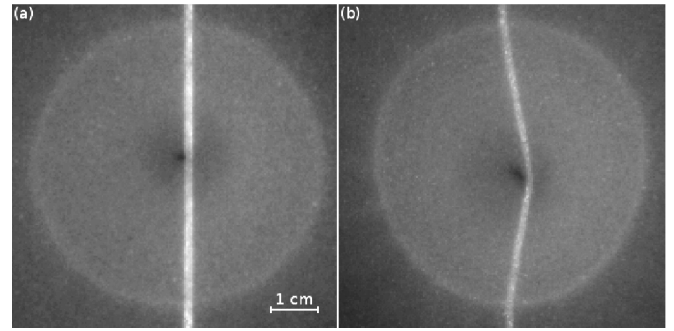


FIG. 2. **Images of the free surface** – (a) Top view – A good contrast is obtained by the use of an annular light source providing an homogeneous grazing light. The bright line is from the vertical light sheet casted onto the surface. (b) Side view – The deformation of the bright line, observed from the side thanks to the second camera makes it possible to reconstruct the surface profile along one radial direction ( $d = 45 - 90 \mu\text{m}$ ,  $D = 6 \text{ mm}$ )

open).

An electronic scale (KERN 440-51N) placed under the container measures the mass  $M$  of the deposited grains with an accuracy to within 0.1 g. The temporal resolution of the measurements is achieved by means of an RS-232 connection to a PC, which makes it possible to record the mass as a function of time at 2 Hz.

The free surface is imaged by means of 2 CCD cameras (JAI CB-080 GE, monitored by CVB 10.0 software from STEMMER IMAGING S.A.S.). The first camera (Fig. 1, camera 1) images the free surface from the top, along the vertical (Fig. 2a). We are interested in observing the vertical deformation of the free surface: A good contrast is achieved by the use of a ring of LEDs, placed slightly above the level of the free surface, which produces an homogeneous grazing light. The second camera (Fig. 1, camera 2) is used to obtain the profile of the free surface in one radial direction. To do so, the latter camera makes an angle of about  $30^\circ$  with respect to the vertical whereas a vertical light-sheet from a LASER diode and a glass cylinder is casted onto the granular surface. In this latter configuration, the profile of the free surface can reconstructed from the deformation of the bright line visible in the image (Fig. 2b). The images from both cameras are recorded during the container discharge and subsequently analyzed with ImageJ [28].

## The granular material

The granular material consists of sodosilicate glass beads (Matrasur, sodosilicate glass, density  $2200 \text{ kg/m}^3$ ). In order to probe different situations, experiments are carried out on seven different granular batches (Table I). For all batches, the measured density of the granular ma-

terial is  $\rho = (1510 \pm 20) \text{ kg/m}^3$ , corresponding to a compacity of about  $0.68 \pm 0.02$ . Using these different batches we expect to observe different behaviors. Indeed, on the one hand, for batches 4 to 7, the granular material flows easily and does not exhibit cohesion. In other words, the beads do not stick significantly to each other. On the other hand, for batches 1 and 2, the granular material is strongly cohesive and any attempt to make the material flow leads to the appearance of fractures. For these batches, the adhesion force between the grains is significant. Finally, batch 3 exhibits an intermediate state (a weak cohesion between beads).

1	2	3	4	5	6	7
0-45	45-90	75-150	150-200	180-300	250-425	425-600
○	○	○/●	●	●	●	●
88	56	34	22	22	22	22

TABLE I. **Granular batches** – Seven different batches, consisting of glass spheres, were used in the experiments. Small grains clearly exhibit cohesion whereas large grains do not exhibit any apparent cohesive behavior. Batch 3 is an intermediate case (Top: batch number. Center : diameter range in  $\mu\text{m}$ . Center : ○ cohesion; ● no apparent cohesion. Bottom : lateral slopes angle  $\theta_c$ .)

Several reasons can explain the cohesion in batches made of small grains. It may originate from capillary bridges between beads due to room humidity [26, 27], or from Van der Waals interactions as well [29, 30]. In our experimental conditions, both reasons are likely to be involved in the cohesion. Whatever the physical origin of the cohesion, it will be accounted for by the measurement of the angle of avalanche,  $\theta_a$ , which indeed depends on the adhesion force between the grains [31].

### Experimental procedures

The experiment is prepared by filling, without any specific care, the container with the granular material up to a height of about 15 cm and by subsequently levelling the free surface in order to start from a flat surface and a well-defined granular height. Acquisitions of the images and of the deposited weight are started a few seconds before the aperture is opened. The experiment finishes once the grains stop flowing. Acquisitions are stopped a few seconds later.

## EXPERIMENTAL RESULTS

### Cohesionless material

In the case of cohesionless material, the discharge process is entirely reproducible involving a discharge at continuous flow-rate and a regular shape of the crater. We

thus first report experimental results obtained for batches 4 to 7, therefore for grain diameters larger than  $150 \mu\text{m}$  typically.

### Discharge rate

For large grains, one observes a linear increase of the deposited mass  $M$  as a function of time  $t$  (Fig 3), and thus a constant flow-rate  $Q$ , thorough the entire discharge: We mention that, on the one hand, the stationary regime is reached immediately after the outlet is opened. On the other hand, a short transitory regime is observed just before the flow stops, at end of the reservoir drainage. Its duration, a few seconds, much less than the duration of the entire discharge, depends on the flow-rate.

In the final state an annular pile remains around the outlet.

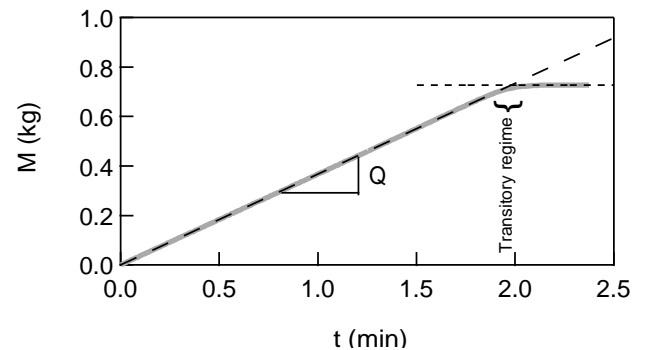


FIG. 3. **Deposited mass  $M$  vs. time  $t$**  – For cohesionless materials, the deposited mass  $M$  increases linearly with time  $t$  thorough the entire discharge. The permanent regime is reached immediately after the outlet is opened and the flow-rate  $Q$  can be accurately determined from the slope. The final transitory regime, during typically 10 seconds in this example, corresponds to the fall of the last grains along the granular slopes that remain around the outlet in the final state ( $d = 250 - 425 \mu\text{m}$ ,  $D = 6 \text{ mm}$ ).

In the whole experimental range of the aperture diameter  $D$ , the experiments are reproducible and the flow rate  $Q$  only depends on the diameters  $d$  and  $D$  of the beads and outlet, respectively. It is particularly interesting to note that the flow-rate  $Q$  is constant even if the granular height above the outlet is smaller than the container diameter: even if the Janssen effect cannot insure that the pressure at the outlet is constant, the flow-rate remains constant [13]. Considering various choices of  $d$  and  $D$  (Fig. 4), we recover that the mass flow-rate  $Q$  is indeed given by the Beverloo law [1, 17]:

$$Q = A \rho g^{\frac{1}{2}} (D - kd)^{\frac{5}{2}} \quad (1)$$

where  $\rho = 1510 \text{ kg/m}^3$  denotes the density of the granular material and  $g$  the acceleration due to the gravity.

From the interpolation of the experimental data we determine the prefactor  $A = 0.63 \pm 0.06$ . As expected from simple geometrical arguments, the size of the aperture is effectively reduced by a constant length of the order of the grain diameter  $d$  and we estimate  $k = 1.0 \pm 0.1$ .

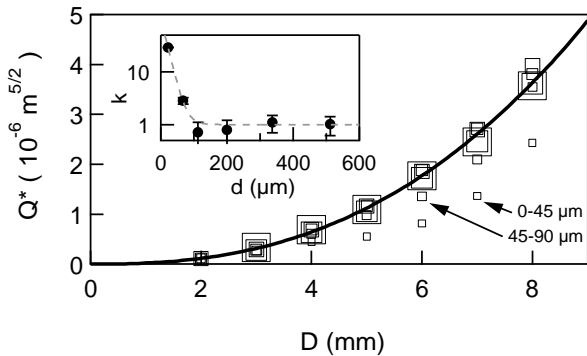


FIG. 4. **Reduced flow-rate  $Q^*$  vs.  $D$**  – We report the reduced flow-rate  $Q^* \equiv Q/[\rho\sqrt{g}(1-d/D)^{2.5}]$  as a function of the aperture diameter  $D$  (The symbol size is proportional to the grain diameter  $d$ ). We observe that, for cohesionless materials (larger grains, batches 4 to 7), the flow-rate is satisfactorily given by Beverloo law (Eq. 1) with  $k = 1.0 \pm 0.1$  and  $A = 0.63 \pm 0.06$  (continuous line). For cohesive grains, the flow-rate varies a lot from one experimental run to another (typically up to 30% in the case of batch 2 and up to 50% for batch 1). In average, the flow-rate is smaller, given by Beverloo law with  $A = 0.63 \pm 0.06$  and larger values of  $k$  that are reported in the inset (error bars of about 10%, barely visible in the log-lin scale used to point out that  $k$  is about 1 for the cohesionless materials).

#### Dynamics of the free surface

For cohesionless materials, soon after the reservoir is opened, a crater forms at the free surface at the vertical of the outlet. The crater is axi-symmetric and the contour observed from above is a circle of radius  $R(t)$ . For all experimental conditions, we observe that the slopes make a constant angle  $\theta_c$  with the horizontal. The grains avalanching continuously along the slope, we deduce that the experimental angle  $\theta_c$  equals, by definition, the dynamical angle of avalanche  $\theta_a$ . We measure to be  $\theta_a = (21.5 \pm 1)$  deg (Fig. 5). Finally, after the discharge, when the lateral piles are at rest, we measure that  $\theta_c$  is slightly smaller, corresponding then, by definition, to the angle of repose  $\theta_r = (19.5 \pm 1)$  deg.

One can easily account for the temporal evolution of the radius of the crater,  $R(t)$ , by considering that the volume of the crater corresponds to the volume of the deposited mass  $M$  that increases linearly with the time  $t$ . Taking into account the flow-rate  $Q$ , the density of the material  $\rho$  and the dynamical angle of avalanche  $\theta_d$ , one

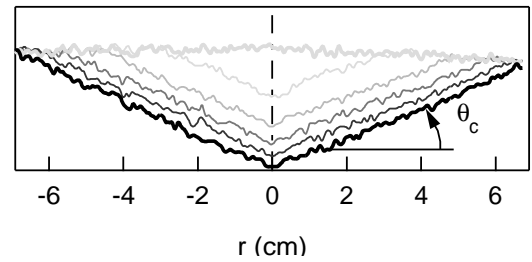


FIG. 5. **Vertical profile at various times  $t$**  – We report the profile of the crater in a vertical plane of symmetry every 5 seconds. We observe that the angle  $\theta_c$  that the slopes make with the horizontal is constant throughout the entire discharge (Thick lines: grey, profile of the initial surface; black,  $t = 25$  s. Thin lines: from light grey to black,  $t = 5$  s to 20 s.  $d = 425 - 600 \mu\text{m}$ ,  $D = 6$  mm).

obtains after simple algebra:

$$R^3(t) = \frac{3Q}{\pi\rho\tan(\theta_c)} t, \quad (2)$$

in good agreement with the experimental data (Fig. 6).

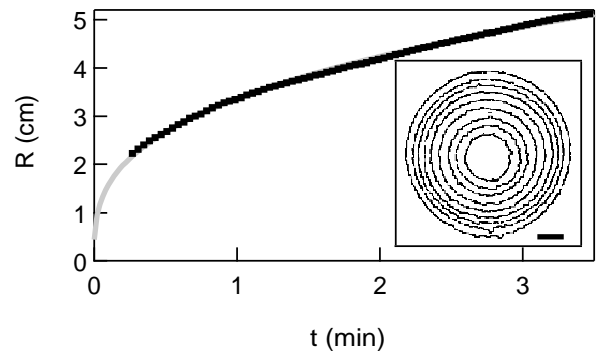


FIG. 6. **Radius  $R$  vs. time  $t$**  – In agreement with  $Q$  constant and simple geometrical arguments,  $R$  scales like  $t^{1/3}$  [Black dots, experimental data; grey line, Eq. (2)]. Inset: contours of the crater in the horizontal plane at different, equally-spaced (2.5 sec), times  $t$  (The scale bar is worth 2 cm.  $d = 150 - 250 \mu\text{m}$ ,  $D = 6$  mm).

In the next section, we will consider the behavior of the flow-rate as well as that of the free surface when the cohesion is involved in the discharge process. We will make use of the results previously reported for the cohesionless material to analyze the phenomenon in the same framework.

#### Cohesive material

For small grains (batches 1 and 2), typically smaller than  $100 \mu\text{m}$ , when cohesion plays a role, one observes

that the discharge leads to the formation of an irregular crater which results from a sequence of independent avalanches. In this case, the experiments are not, strictly speaking, reproducible. From one experiment to another, the discharge process may vary a lot. In particular, the quantity of granular material that fell through the orifice during the reservoir drainage can be very different for two experiments performed in the same experimental conditions (same grains and same outlet diameter  $D$ ). In practice, we note variations of the average flow rate  $Q$  of about 30% in the case of batch 2 ( $d = 45 - 90 \mu\text{m}$ ) and of about 50% for the smallest grains (batch 1,  $d = 0 - 45 \mu\text{m}$ ), from one experimental run to another. This may come from the difficulty of preparing identical initial states. Indeed, the way the beads are poured in the tank significantly affects the initial compaction, and thus the discharge process, of cohesive granular materials. Nevertheless, the typical behavior of the material during the discharge exhibits several common features that we report in the present section.

#### Discharge rate

Although the dynamics is intermittent at the free surface, the mass of granular material flowing out through the hole still exhibits a linear increase, with little fluctuations, as a function of time thorough the entire discharge (Fig. 7). Therefore, as for cohesionless material,  $Q$  is constant. In this case again, the flow rate, which depends on the diameters  $d$  and  $D$  of the grains and of the outlet respectively, is independent of the amount of material above.

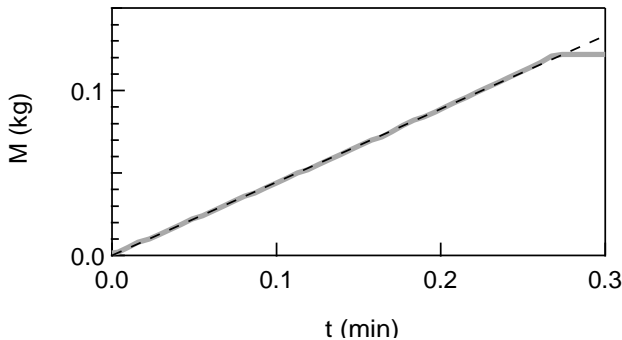


FIG. 7. **Deposited mass  $M$  vs. time  $t$**  – For cohesive materials, the deposited mass  $M$  increases linearly with time  $t$  thorough the entire discharge in spite of the intermittent avalanche process occurring in the container ( $d = 45 - 90 \mu\text{m}$ ,  $D = 6 \text{ mm}$ ).

It is particularly interesting to point out that, surprisingly, the flow rate is constant in spite of the intermittent dynamics of the avalanche process above. The explanation of such behavior is found by direct observation of

the crater. Indeed, one easily observes that the drainage involves two different processes. First, the grains that detach from the lateral slopes fall down in the crater. This fluidized material flows continuously through the outlet. Second, the decrease of the height of fluidized material in the crater leads to a destabilization of the lateral walls of the crater. The resulting avalanches feed, in turn, the fluidized region above the outlet. The flow rate which does not depend on the height of grains above the outlet remains constant.

For cohesive grains, the experimental flow-rate  $Q$  is observed to be significantly smaller than that expected with the values  $A = 0.63$  and  $k = 1$  (cohesionless samples) in Beverloo law (Fig. 4). However, the experimental data from the cohesive samples are correctly accounted for by Eq. 1 with  $A = 0.63 \pm 0.06$  ( $\forall d$ ), but with  $k$  increasing with the cohesive nature of the material (small grain size, Fig. 4, inset). This might be because the cohesion is only partially destroyed when the grains flow. Due to the remaining cohesion, grain aggregates, rather than individual grains, flow out through the aperture. In this case, the effective diameter  $d_{\text{eff}}$  of the falling grains is larger than the individual grain diameter  $d$ , leading to a smaller effective outlet diameter [ie to a larger value of  $k$  in Beverloo law (1)].

It is particularly interesting to comment here the measurements of the flow rate, even if they were not the scope of the present article. Indeed, the fact that the  $Q$  is constant throughout a silo discharge is not an obvious result. In the litterature, the constancy of  $Q$  has been often implicitly assumed to be a result of the so-called Janssen effect, a saturation of the pressure at the base of a static silo. Indeed, in this case, the pressure in the outlet region would be constant, independant of the height of material above. Even if the authors generally did not explicitly state that there was a relation between the constancy of the flow-rate and the Janssen effect, they made erroneously think that the flow-rate was constant because the pressure in the outlet region was constant. Note first that the Janssen effect is a static effect and that there is no reason for the pressure to be constant when the material is flowing. We now know that, indeed, the pressure is not constant during the discharge, as proven by direct measurements of the forces exerted by the material on the container [24, 32]. Moreover, in Ref. [32], the authors show that the flow rate is not altered by vibrations of the container that avoid static arching. Independently, it has been proven in a horizontal system (a conveyor belt) that the flow-rate does not depend on the pressure and obeys Beverloo law, the typical velocity at the outlet to consider in this case being the belt velocity instead of the free fall velocity  $\sqrt{gD}$  [13]. Our experiment interestingly provides an additional experimental proof of the same assertion, the flow-rate being constant even if the height of the granular column is never larger than the radius of the container. The pressure surely varies dur-

ing the discharge but  $Q$  is constant and accounted for by Beverloo law. Furthermore, we observe that the cohesion mainly alters,  $k$ , thus the typical size of the particles to be considered; the size of grain aggregates rather than the diameter of individual grains.

The physical process leading to the reduction of the flow rate being out of the scope of the present article, we do not discuss further this point and focus now on the dynamics of the crater.

#### Dynamics of the free surface

For cohesive material, the crater geometry and dynamics are noticeably different than those reported for the cohesionless case.

First, we observe a significant delay between the beginning of the discharge and the appearance of a crater at the free surface. Because of the cohesion, the material can sustain a cavity at the vertical of the outlet and the deformation of the free surface result from the granular flow at the bottom only when a significant amount of grains has flown out. Once the crater appears at the free surface, the angle that the lateral slopes make with the horizontal is large (Fig. 8). Note that, as the grains at the lateral slopes are not flowing, the crater angle  $\theta_c$  does not correspond to the dynamical angle of avalanche anymore. We also point out that the crater angle does not depend on the diameter  $D$  of the outlet. However, contrary to what is observed for non-cohesive grains, the angle depends on the grain size  $d$ , *i.e.* on the cohesion (Table I): From the vertical profiles of the crater (Fig. 8), we obtain, for instance,  $\theta_c = (88 \pm 2)$  deg for batch 1 (0 - 45  $\mu\text{m}$ ) and  $\theta_c = (56 \pm 1)$  deg for batch 2 (45 - 90  $\mu\text{m}$ ). In agreement with the expectation of a larger effect of the cohesion force on the smaller grains, the angle of avalanche significantly increases when the grain size is decreased [31]. From now on, we shall consider the crater angle  $\theta_c$  as the quantity accounting for the cohesion.

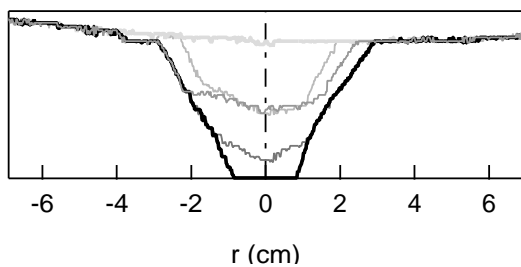


FIG. 8. **Vertical profile at various times  $t$**  – We report the profile of the crater in a vertical plane every 5 seconds. We observe that the slopes on the side are much steeper than in the cohesionless case (Thick lines: grey, profile of the initial surface; black,  $t = 20$  s. Thin lines: from light grey to black,  $t = 5$  s to 15 s.  $d = 45 - 90 \mu\text{m}$ ,  $D = 6$  mm).

As mentioned above, the crater is no more circular and its growth is due to successive, partial, collapses of the lateral walls. This behavior is clearly revealed by the dynamics of the contours obtained from the images from top (Fig. 9, inset). The superposition of the contours at several equally-spaced times reveals that the intermittent nature of the discharge. In such an image, in which the superposition of the contours draws a "flower" at the surface, one directly observes that the size of the avalanches and the delay (lines are darker away from the center) between successive events increase with time. In order to report quantitative results, we define the average radius  $R$  of the crater,  $R \equiv \sqrt{A/\pi}$ , where  $A$  is the surface area of the crater in the horizontal plane. Reporting  $R$  as a function of time (Fig. 9), we observe that  $R$  increases by jumps, each corresponding to a partial collapse of the lateral wall. Again, the results point out that both the typical size of the avalanches and the delay between them increase throughout the discharge process. In addition, one observes, in average, the scaling  $R \propto t^{1/3}$ , which is compatible with a constant flow-rate and constant angle  $\theta_c$  of the lateral walls.

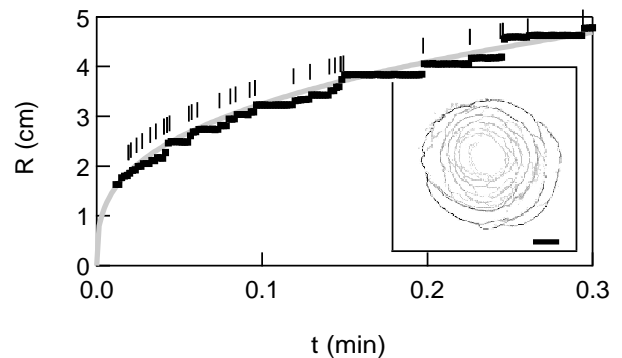


FIG. 9. **Effective radius  $R$  of the crater vs time  $t$**  – The average radius of the crater increases by independent jumps. However, in average,  $R$  scales like  $t^{1/3}$ . The vertical dashes mark the avalanche events observed directly in the images [Black dots, experimental data; grey line, Eq. 2 with  $\theta_c = 56$  deg,  $\rho = 1510 \text{ kg/m}^3$  and the measured dimensionless flow-rate  $Q^* = 1.75$ ]. Inset: superposition of the crater contours in the horizontal plane at different, equally-spaced, times  $t$ . The darker the line is, the longer the contour remained at the given position (The scale bar is worth 2 cm.  $d = 45 - 90 \mu\text{m}$ ,  $D = 6$  mm).

#### Geometrical characterization of the "flower"

To characterize further the discharge process, we now characterize the geometry of the crater seen from above. In particular, we observe that, during the discharge process, the typical size (arc length) of the avalanches increases with the distance to the center so that one can

consider the angular size of the avalanche,  $\alpha$  (the angle that the straight lines joining the centre to the two ends of the avalanche make between them, Fig. 10). Such an analysis is possible only when the material is sufficiently cohesive so that one can distinguish individual avalanches, thus for the smallest grains. We thus report results obtained for batches 1, 2 and 3, only.

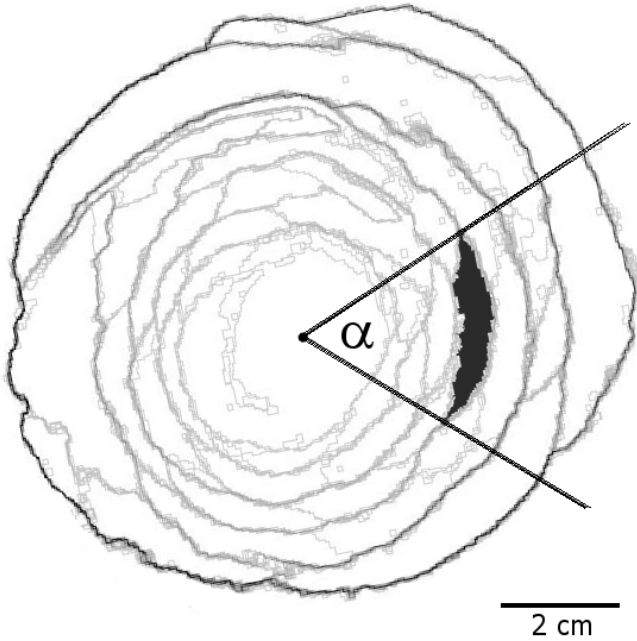


FIG. 10. **Geometrical characterization of the "flower"** – We determine the angular size  $\alpha$  of each of the individual avalanches ( $d = 45 - 90 \mu\text{m}$ ,  $D = 6 \text{ mm}$ ).

We thus consider the distribution of  $\alpha$  measured throughout several discharges (typically, 200 to 300 avalanches). We observe that the distributions of  $\alpha$  do not depend significantly on the aperture diameter  $D$  and report results obtained for  $D = 6 \text{ cm}$  (Fig. 11). The distributions are broad and asymmetric but we note that the typical angular size is significantly larger for the smaller grains. For instance, the experimental results lead to  $\alpha = (73 \pm 23) \text{ deg}$  for  $d = 0 - 45 \mu\text{m}$  and  $\alpha = (54 \pm 17) \text{ deg}$  for  $d = 45 - 90 \mu\text{m}$  (Fig. 11). For the cohesionless samples such an estimate cannot be obtained whereas for the intermediated case  $d = 75 - 150 \mu\text{m}$  the individual avalanches can barely be isolated and we can only get an estimate  $\alpha = 17 \text{ deg}$  with an error of about 100 % (Fig. 12). We observe that  $\alpha \rightarrow 0$  for vanishing small cohesion ( $\theta_c = 22 \text{ deg}$ ), which can be understood by considering that the continuous collapse of the walls in this case consists in an infinite number of infinitely small avalanches.

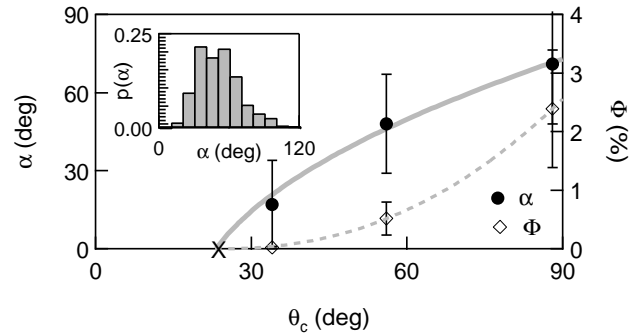


FIG. 11. **Angular size  $\alpha$  and parameter  $\Phi$  vs crater angle  $\theta_c$**  – The typical angular size of the avalanches,  $\alpha$  and the parameter  $\Phi$  (Eq. 4) increase significantly with the typical angle  $\theta_c$  that the lateral walls make with the horizontal, thus with the cohesion (The cross indicates  $\theta_c = 22 \text{ deg}$  for cohesionless batches and the continuous lines are only a guide to the eyes). Inset: Distribution  $p(\alpha)$  for  $d = 45 - 90 \mu\text{m}$  ( $D = 6 \text{ mm}$ ).

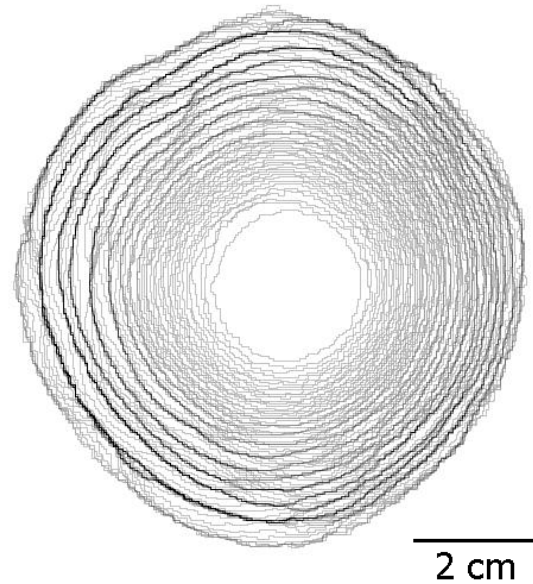


FIG. 12. **Dynamics of the interface for an intermediate case** – When the sample is almost cohesionless, the individual avalanches can barely be isolated even if the dynamics is clearly intermittent. The discharge involves a series of small avalanches that propagate along the crater walls ( $d = 75 - 150 \mu\text{m}$ ,  $D = 6 \text{ mm}$ ).

#### *Additional characterization of the discharge dynamics*

In order to characterize further the intermittent nature of the discharge, we define an estimate,  $M(t)$ , of the mass of material that fell down the slopes at time  $t$ . To do so, we use the apparent radius  $R(t)$  and the angle  $\theta_c$

of the crater and write, considering the volume of the corresponding cone,

$$M = \rho \frac{\pi R^3}{3} \tan(\theta_c). \quad (3)$$

Then, from the estimated mass  $M(t)$  and the actual mass  $m(t)$  that is directly measured with the balance, we define:

$$\Phi = \frac{1}{T m_\infty^2} \int_0^T [m(t) - M(t)]^2 dt \quad (4)$$

where  $T$  stands for the total duration of the discharge and  $m_\infty$  for the total mass of material measured after the discharge. The parameter  $\Phi$  accounts for the intermittent nature of the discharge. Indeed,  $M(t) = m(t)$  and thus  $\Phi = 0$  for a cohesionless material. For cohesive materials, due to the avalanches at the free surface, the temporal fluctuations in  $R$  (and thus in  $M$ ) are enhanced whereas the flow rate is constant and  $m$  increases linearly with time. Thus,  $\Phi$  is expected to increase with the intermittent nature of the discharge process and, thus, to account for the cohesion. In the figure 11, we report the experimental values of  $\Phi$  as a function of the crater angle  $\theta_c$ . We note that, even if it, indeed, increases significantly for the cohesive sample,  $\Phi$  gently vanishes for vanishing cohesion: the occurrence of small avalanches observed in the case of batch 3 does not produce any important oscillation of the estimated mass  $M(t)$  and the parameter  $\Phi$  is not very appropriate to reveal the cohesive nature of the material. The measure of the angular size  $\alpha$  is much more efficient for this purpose as it significantly depends on the crater angle  $\theta_c$  even for almost cohesionless materials.

## DISCUSSION AND CONCLUSION

The experimental results can be summarized as follows: for large enough aperture, the discharge is continuous in the sense that the flow rate is constant throughout the discharge. The results holds true in absence or presence of cohesion. However, when the material is (even weakly) cohesive, the dynamics of the free surface is intermittent. Instead of an axi-symmetric conical crater, one observes an irregular crater which results from a series of individual avalanches. The typical size of the avalanches increases with the crater size, which permits to define, for a given material, an angular size which increases with the cohesion. These results suggest that there is a geometry-based relation between the angular size of the avalanche and the angle that the crater walls make with the horizontal. However, we have not been able to establish this relation theoretically.

In the effort to understand, from the fundamental point of view, the mechanisms governing the discharge of cohesive materials, the present work shall be extended

to measurements of the forces exerted on the base plane and on the wall while tuning the cohesion.

- 
- [1] W.A. Beverloo, H.A. Leninger, and J. van de Valde, *Chem. Eng. Sci.* **15**, 260 (1961).
  - [2] L.P. Kadanoff, *Rev. Mod. Phys.* **71**, 435 (1999).
  - [3] P.G. de Gennes, *Rev. Mod. Phys.* **71**, S374-S382 (1999).
  - [4] V. Trappe, V. Prasad, L. Cipelletti, P. N. Serge, and D. A. Weitz, *Nature (London)* **411**, 772 (2001).
  - [5] H. M. Jaeger, S. R. Nagel, and R. P. Behringer, *Rev. Mod. Phys.* **68**, 1259 (1996).
  - [6] J. Duran, *Sands, Powders and Grains* (Springer, New York, 2000).
  - [7] G. H. Ristow, *Pattern Formation in Granular Materials* (Springer, New York, 2000).
  - [8] R. M. Nedderman, U. Tüzün, S. B. Savage, and G. T. Houlsby, *Chem. Eng. Sci.* **37**, 1597 (1982).
  - [9] U. Tüzün, G. T. Houlsby, R. M. Nedderman, and S. B. Savage, *Chem. Eng. Sci.* **37**, 1691 (1982).
  - [10] S. B. Savage, R. M. Nedderman, U. Tüzün, and G. T. Houlsby, *Chem. Eng. Sci.* **38**, 189 (1983).
  - [11] B. P. Tighe and M. Sperl, *Granular Matter* **9**, 141 (2007).
  - [12] See, for example, R. L. Brown and J. C. Richards, *Trans. 78 Inst. Chem. Eng.* **38**, 243 (1960), comment on p. 167; H. M. Jaeger and S. R. Nagel, *Science* **255**, 1523 (1992), comment on p. 1527; H. M. Jaeger, S. R. Nagel, and R. P. Behringer, *Rev. Mod. Phys.* **68**, 1259 (1996), comment on p. 1261.
  - [13] M.A. Aguirre, J.G. Grande, A. Calvo, L.A. Pugnali and J.-C. Géminard, *Phys. Rev. Lett.* **104**, 238002 (2010).
  - [14] C. Mankoc, A. Janda, R. Arevalo, J. M. Pastor, I. Zuriguel, A. Garcimartín, and D. Maza, *Granular Matter* **9**, 407 (2007).
  - [15] C. Mankoc, A. Garcimartín, I. Zuriguel, D. Maza, and L. A. Pugnali, *Phys. Rev. E* **80**, 011309 (2009).
  - [16] F. Ulissi, graduation thesis, Mechanical Engineering, 2008. Facultad de Ingenieria, University of Buenos Aires, Argentina.
  - [17] R. L. Brown and J. C. Richards, *Principles of Powder Mechanics* (Pergamon Press, Oxford, 1970).
  - [18] Z. Fournier *et al.*, *J. Phys. Condens. Matter* **17**, S477 (2005).
  - [19] M. Scheel *et al.*, *Nature Mater.* **7**, 189 (2008).
  - [20] K. Taylor, P. J. King, and Michael R. Swift, *Phys. Rev. E* **78**, 031304 (2008).
  - [21] N. Olivi-Tran, N. Fraysse, P. Girard, M. Ramonda, D. Chatain, *Eur. Phys. J. B* **25**, 217 (2002).
  - [22] H. Gayvallet and J.-C. Géminard, *Eur. Phys. J. B.* **30**, 369-375 (2002).
  - [23] H. Alarcón, O. Ramos, L. Vanel, F. Vittoz, F. Melo and J.-C. Géminard, *Phys. Rev. Lett.* **105**, 208001 (2010).
  - [24] H. Ahn *et al.*, *Powder Tech.* **186**, 65-71 (2008).
  - [25] A. Janda *et al.*, *Phys. Rev. E* **79**, 031302 (2009).
  - [26] L. Bocquet, E. Charlaix, S. Ciliberto and J. Crassous, *Nature* **396**, 735-737 (1998).
  - [27] S. Nowak, A. Samadani and A. Kudrolli, *Nature Physics* **1**, 50-52 (2005).
  - [28] W.S. Rasband, ImageJ, U. S. National Institutes of Health, Bethesda, Maryland, USA,

<http://rsb.info.nih.gov/ij/>, 1997-2009.

- [29] H. C. Hamaker, *Physica Amsterdam* **4**, 1058 (1937).
- [30] R.Y. Yang *et al.*, *Phys. Rev. E* **78**, 031302 (2008).
- [31] F. Restagno, L. Bocquet, and E. Charlaix, *Eur. Phys. J. E* **14**, 177-183 (2004).
- [32] H. Pacheco-Martinez, H. J. van Gerner and J. C. Ruiz-Surez, *Phys. Rev. E* **77**, 021303 (2008).